Monthly Notices of the ROYAL ASTRONOMICAL SOCIETY

MNRAS **510,** 2572–2582 (2022) https://doi.org/10.1093/mnras/stab3575
Advance Access publication 2021 December 14

Pulsar death line revisited – I. Almost vacuum gap

V. S. Beskin[1,2]★ and P. E. Litvinov[2]

[1]*P.N.Lebedev Physical Institute, Leninsky prosp., 53, Moscow, 119991, Russia*
[2]*Moscow Institute of Physics and Technology, Dolgoprudny, Moscow region, Institutsky per. 9, 141700, Russia*

Accepted 2021 December 3. Received 2021 October 23; in original form 2021 June 18

ABSTRACT

In this paper, which is the first in a series of papers devoted to a detailed analysis of 'the death line' of radio pulsars, we consider a possibility of producing secondary particles at a sufficiently long pulsar period P. To this end, we reconsidered the potential drop necessary for secondary plasma generation in the inner gap over magnetic polar caps. Our research made it possible to refine the conditions for generating secondary plasma, such as the multiplicity of the production of secondary particles and their spatial distribution. Our research also made it possible to further quantitatively analyse the dependence of the possibility of secondary plasma generation on all parameters, including the inclination angle of the magnetic axis to the rotation axis, the polar cap size and the magnetic field geometry.

Key words: pulsars: general – stars: neutron.

1 INTRODUCTION

According to our modern understanding of the phenomenon of radio pulsars, their radio emission is associated with secondary electron–positron plasma generated in the polar regions of a neutron star (Sturrock 1971; Ruderman & Sutherland 1975; Arons 1982; Lorimer & Kramer 2012; Lyne & Graham-Smith 2012). It is therefore not surprising that the cessation condition of the generation of secondary particles is associated with the so-called 'death line' on the P–$\dot{P}$ (or P–B_0) diagram, where P is the pulsar period, and B_0 is the magnetic field at the magnetic pole.

Detailed works devoted to the generation of secondary plasma have been underway since the beginning of the eighties (Daugherty & Harding 1982; Gurevich & Istomin 1985; Arendt & Eilek 2002; Istomin & Sobyanin 2007; Medin & Lai 2010; Timokhin 2010; Timokhin & Arons 2013; Philippov, Spitkovsky & Cerutti 2015; Timokhin & Harding 2015; Cerutti, Philippov & Spitkovsky 2016). Nevertheless, up to now, a large number of different options are discussed in the literature (Ruderman & Sutherland 1975; Blandford & Scharlemann 1976; Arons 1982; Usov & Melrose 1995), leading to very different conditions which set 'the death line' of radio pulsars (Chen & Ruderman 1993; Zhang, Harding & Muslimov 2000; Hibschman & Arons 2001; Faucher-Giguére & Kaspi 2006; Konar & Deka 2019).

In this and the following article, we set ourselves the task of reconsidering all basic approximations usually used in constructing the secondary plasma production model, but which may work poorly near 'the death line'. In particular, we assume that due to irregularity of the secondary plasma production, almost the entire region of open field lines can be considered in a vacuum approximation: $\rho_e = 0$. In other words, our task is to clarify the position of 'the death valley' (Chen & Ruderman 1993) using modern models of the magnetosphere structure and the deceleration of a neutron star; the latter is necessary to quantify the period derivative $\dot{P}$ in terms of P, B_0, and the inclination angle χ. The effects of general relativity will also be taken into account.

Please note that in this work, the 'classical' mechanism of the particle production is considered due to the single-photon conversion of the γ-quantum into an electron–positron pair in a superstrong magnetic field. As is well known (Sturrock 1971; Ruderman & Sutherland 1975), this process includes primary particle acceleration by a longitudinal electric field, emission of γ-quanta due to curvature radiation, production of secondary electron–positron pairs, and, finally, secondary particle acceleration in the opposite direction, which also leads to the creation of secondary particles. In other words, we do not consider particle production due to Inverse Compton Scattering, which, as is well known (Blandford & Scharlemann 1976; Zhang et al. 2000), can also be a source of hard γ-quanta. As an excuse, we note that we will first of all be interested in old pulsars, in which the surface temperature may not be high enough to form a sufficient number of X-ray photons.

For the same reason, we do not take into consideration synchrotron photons emitted by secondary pairs. The point is that, as is well known (see, e.g. Gurevich & Istomin 1985; Istomin & Sobyanin 2007 and section 3.1 below), the energy of synchrotron photons emitted by secondary particles is approximately 15–20 times less than the energy of curvature photons emitted by primary particles. Therefore, near the threshold of particle production, when the free path length of curvature photons become close to the radius of the star R, the pulsar magnetosphere appears to be transparent for synchrotron photons.

Let us recall that the cessation condition for the pair creation determining 'the death line' was first evaluated by Ruderman & Sutherland (1975) from the equality of the height of the 1D vacuum gap

$$H_{\rm RS} \sim \left(\frac{\hbar}{m_e c}\right)^{2/7} \left(\frac{B_0}{B_{\rm cr}}\right)^{-4/7} R_{\rm L}^{3/7} R_{\rm c}^{2/7} \qquad (1)$$

and the polar cap radius

$$R_{\rm cap} \approx \left(\frac{\Omega R}{c}\right)^{1/2} R. \qquad (2)$$

★ E-mail: beskin@lpi.ru

Here $B_{\rm cr} = m_{\rm e}^2 c^3/e\hbar = 4.4 \times 10^{13}$ G is the Schwinger magnetic field, $R_{\rm L} = c/\Omega$ is the radius of the light cylinder ($\Omega = 2\pi/P$ is the star angular velocity) and $R_{\rm c}$ is the curvature of the magnetic field lines near the magnetic pole. For the magneto-dipole energy losses

$$W_{\rm tot} \sim \frac{B_0^2 \Omega^4 R^6}{c^3} \tag{3}$$

and the dipole magnetic field stricture, when

$$R_{\rm c} = \frac{4}{3}\frac{r}{\theta_m}, \tag{4}$$

(r and θ_m are the polar coordinates relative to the magnetic axis, r is the distance from the star center), one can obtain for 'the death line' (Ruderman & Sutherland 1975)

$$\dot{P}_{-15} = \beta_{\rm d} P^{11/4}, \tag{5}$$

where $\dot{P}_{-15} = 10^{15}\dot{P}$ and $\beta_{\rm d} \sim 1$.

It is clear that in the mid 70s, such accuracy was quite acceptable, especially since expression (5) was really limited from below most of the pulsars in the P–$\dot{P}$ diagram. However, as was already shown by Chen & Ruderman (1993), the standard RS model (dipole magnetic field, etc.) gives a very large period derivative $\dot{P}$ for the observed 'death line'. That is why the idea was put forward to consider a more complex structure of the magnetic field resulting in a decrease of the period derivative (and leading to the appearance of 'a death valley'). However, as was already emphasized, the observed period derivative $\dot{P}$ can be affected by many other reasons (masses and radii of neutron stars, the size of the polar cap, the effects of general relativity), which were not considered in the qualitative analysis carried out by Chen & Ruderman (1993). In particular, within the framework of this model, the simplest magnetodipole formula was used to determine the period derivative $\dot{P}$, which, as it is now clear, does not correspond to reality. Therefore, one of the main tasks of our consideration is the question of what parameters can lead to a decrease in the observed deceleration rate $\dot{P}$.

To clarify this issue, we consider an almost vacuum gap model of the polar region. Remember that all modern models of particle generation (including recent PIC simulations) implicitly assume free ejection of particles from the neutron star surface. Consequently, one could expect that the potential drop would be close to that predicted in the Arons (1982) model, i.e. much smaller than in the vacuum gap Ruderman–Sutherlend model. However, as was shown in recent works performed in the PIC simulation (Timokhin 2010; Philippov, Timokhin & Spitkovsky 2020), due to strong non-stationarity, vacuum regions appear from time to time, with the potential drop being close to the vacuum gap model. Particularly, such an assumption is natural for the pulsars located near 'the death line'. In this case, the beginning of the cascade (and, hence, the filling of this region with a secondary electron–positron plasma) can be initiated by the cosmic gamma background, which, as is known, leads to 10^5–10^8 primary particles per second in the polar cap region (Shukre & Radhakrishnan 1982).

On the other hand, for the pulsars in the vicinity of 'the death line', the free path length l_γ of γ-quanta leading to the production of secondary particles can be of the order of star radius R (the scale of the diminishing of the dipole magnetic field), i.e. much larger than the transverse size of the polar cap $R_{\rm cap} \sim 0.01R$. Therefore, we need to determine 3D potential resulting in the acceleration of primary particles.

Let us note straight away that below we consider only a dipole magnetic field despite a large number of works which indicated that it is impossible to explain 'the death line' in a dipole magnetic field (Arons 1993; Asseo & Khechinashvili 2002; Barsukov & Tsygan 2010; Igoshev, Elfritz & Popov 2016; Bilous et al. 2019). In other words, one of our tasks is to verify the possibility of explaining the position of 'the death line' by other factors which are usually not considered when analysing the processes of secondary plasma production. Among such possible factors, one can indicate a decrease in the magnetic field with distance from the star, the possibility of producing secondary pairs by γ-quanta whose energy is much larger than the typically used characteristic energy of the maximum of the spectrum, as well as the fact that secondary plasma is generated on field lines located closer to the magnetic axis than gamma-ray emitting particles. All these effects become significant near 'the death line' when the free pass length of γ-quanta becomes comparable to the radius of a neutron star. The role of the non-dipole magnetic field and all the other physical parameters which can affect the position of 'the death line', will be discussed in detail in Paper II.

As for Paper I, which is the first in a series of papers devoted to a detailed analysis of 'the death line' of radio pulsars, it is devoted to the possibility of producing secondary particles at sufficiently large periods P. In Section 2, we construct an exact three-dimensional solution for a longitudinal electric field $E_\parallel$ in the polar regions of a neutron star in the case when plasma is absent in the entire region of open field lines. We show that in real dipole geometry for non-zero inclination angles χ, the longitudinal electric field decreases much slower than previously assumed. In addition, the corrections related to the effects of general relativity are determined. Further in Section 3, we show that close to 'the death line' a major role in particle creation begin to play those γ-quanta whose energy is several times greater than the commonly used characteristic energy of curvature radiation. Finally, in Section 4, the generation of secondary electron–positron pairs near 'the death line' is considered when the second-generation particles produced by the conversion of synchrotron photons can be neglected. Section 5 is devoted to the conclusion and discussion.

2 ALMOST VACUUM GAP

2.1 Potential drop

To begin with, we revise the electric potential ψ over the polar cap assuming that near 'the death line', almost all plasma goes away so that one can put $\rho_{\rm e} = 0$ everywhere within the open magnetic field line region. As in the rotation reference frame, the first Maxwell equation has a form (Ruderman & Sutherland 1975)

$$\nabla \boldsymbol{E} = 4\pi(\rho_{\rm e} - \rho_{\rm GJ}), \tag{6}$$

where

$$\rho_{\rm GJ} = -\frac{\boldsymbol{\Omega B}}{2\pi c} \tag{7}$$

is the Goldreich & Julian (1969) charge density, the electric potential ψ must satisfy the relation

$$\nabla^2\psi = -2\frac{\boldsymbol{\Omega B}}{c} \tag{8}$$

with the boundary conditions

$$\psi(\text{star surface}) = 0, \tag{9}$$

$$\psi(\text{separatrix}) = 0. \tag{10}$$

As is well known (see, e.g. Beskin 2010 for more detail), the first boundary condition is related to the assumption of the high conductivity of a neutron star surface. The second condition on

the separatrix separating the regions of open and closed field lines follows from the assumption that in the closed field line region, there is enough plasma to screen the longitudinal electric field. Note also that, despite the fact that the shape of the polar cap is not circular at non-zero inclination angles, we restrict ourselves to considering only the case of a circular polar cap.

In real dipole geometry, when $\boldsymbol{B} = [3(\boldsymbol{nm})\boldsymbol{n} - \boldsymbol{m}]/r^3$, equation (8) looks like

$$\frac{1}{r^2}\frac{\partial}{\partial r}\left(r^2\frac{\partial\psi}{\partial r}\right) + \frac{1}{r^2\sin\theta}\frac{\partial}{\partial\theta}\left(\sin\theta\frac{\partial\psi}{\partial\theta}\right) + \frac{1}{r^2\sin^2\theta}\frac{\partial^2\psi}{\partial\varphi^2} = -2\frac{\Omega B_0}{c}\frac{R^3}{r^3}\left(\cos\theta\cos\chi + \frac{3}{2}\sin\theta\sin\varphi\sin\chi\right), \quad (11)$$

where χ is the inclination angle. Then for the circular shape of the polar cap, the boundary conditions (9)–(10) have a form

$$\psi(r = R, \theta, \varphi) = 0, \quad (12)$$

$$\psi(r, \theta = \theta_0(r), \varphi) = 0, \quad (13)$$

where for small angles θ

$$\theta_0(r) = \left(\frac{rR_0^2}{R^3}\right)^{1/2}. \quad (14)$$

Here

$$R_0 = f_*^{1/2}\left(\frac{\Omega R}{c}\right)^{1/2} R \quad (15)$$

is the polar cap radius, and we introduce standard dimensionless area $f \sim 1$.

For zero longitudinal electric currents, the dimensionless area of a polar cap f_* changes from $f_* = 1.59$ for $\chi = 0^\circ$ to $f_* = 1.96$ for $\chi = 90^\circ$ (Michel 1973; Beskin, Gurevich & Istomin 1983). Modern numerical simulations show that f_* changes from $f_* = 1.46$ for $\chi = 0^\circ$ to $f_* = 1.75$ for $\chi = 90^\circ$ (Gralla, Lupsasca & Philippov 2017). The convenience of introducing a dimensionless area f is due to the fact that in a dipole field for small angles,

$$\theta = f^{1/2}\left(\frac{\Omega r}{c}\right)^{1/2}, \quad (16)$$

so that f is constant along the dipole magnetic field line.

As a result, the solution of equation (11) looks like

$$\psi = \frac{1}{2}\frac{\Omega B_0 R_0^2}{c}\cos\chi \times \left[1 - \frac{\theta^2}{\theta_0^2(r)} - \sum_i c_i^{(0)}\left(\frac{r}{R}\right)^{-\lambda_i^{(0)}/\theta_0'} J_0\left(\lambda_i^{(0)}\theta/\theta_0'\right)\right] + \frac{3}{8}\frac{\Omega B_0 R_0^2}{c}\sin\varphi\sin\chi \times \left[\theta - \frac{\theta^3}{\theta_0^2(r)} - \theta_0'\sum_i c_i^{(1)}\left(\frac{r}{R}\right)^{-\lambda_i^{(1)}/\theta_0'} J_1\left(\lambda_i^{(1)}\theta/\theta_0'\right)\right]. \quad (17)$$

Here

$$\sum c_i^{(0)} J_0\left(\lambda_i^{(0)}x\right) = 1 - x^2 \quad (18)$$

and λ_i are the zeros of the Bessel function $J_0(x)$:

$$\lambda_1^{(0)} = 2.4,\ \lambda_2^{(0)} = 5.5,\ \lambda_3^{(0)} = 8.65,\ \lambda_4^{(0)} = 11.8, \ldots \quad (19)$$

Accordingly, $\lambda_i^{(1)}$ are the zeros of the Bessel function $J_1(x)$:

$$\lambda_1^{(1)} = 3.8,\ \lambda_2^{(1)} = 7.0,\ \lambda_3^{(1)} = 10.2,\ \lambda_4^{(1)} = 13.3, \ldots \quad (20)$$

and

$$\sum c_i^{(1)} J_1\left(\lambda_i^{(1)}x\right) = x - x^3. \quad (21)$$

Since all the terms under the sum signs in (17) rapidly decrease with increasing r, we put here $\theta_0' = \theta_0(R) = \text{const}$.

It is instructive to stress that for the symmetric (φ-independent) part, one can obtain

$$\sum c_i^{(0)} = 1, \quad (22)$$

$$\sum c_i^{(0)}\left(\lambda_i^{(0)}\right)^2 J_0(\lambda_i x) = 4, \quad (23)$$

the last condition resulting from (8). In particular, for $x = 0$, we have

$$\sum c_i^{(0)}\left(\lambda_i^{(0)}\right)^2 = 4. \quad (24)$$

Unfortunately, the second series (23) converges very slowly (see Appendix A). For this reason, in what follows, we restrict ourselves to only the first four terms $c_i^{(0)}$ for which the coefficients $c_1^{(0)}$ and $c_2^{(0)}$ coincide with the precisely calculated values, and the two remaining ones are selected to satisfy relations (22) and (24). As a result, we obtain

$$c_1^{(0)} = 1.09,\ c_2^{(0)} = -0.11,\ c_3^{(0)} = 0.028,\ c_4^{(0)} = -0.0075, \quad (25)$$

so that $\sum c_i^{(0)} = 1.00$ and $\sum c_i^{(0)}(\lambda_i^{(0)})^2 = 4.03$. As shown in Appendix A, in some respects, these four terms (25) approximate the constant (23) even better than twenty exact coefficients $c_i^{(0)}$; in particular, the sum of the first twenty terms of the series (24) results in 3.37 instead of 4.

Accordingly, for anti-symmetric (φ-dependent) part, equation (8) gives

$$\sum c_i^{(1)}\left(\lambda_i^{(1)}\right)^3 J_1(\lambda_i x) = 8x. \quad (26)$$

Together with (21) in the limit $x \to 0$ it gives

$$\sum c_i^{(1)}\lambda_i^{(1)} = 2, \quad (27)$$

$$\sum c_i^{(1)}\left(\lambda_i^{(1)}\right)^3 = 16. \quad (28)$$

Restricting ourselves to the four terms of the series, we again determine the first two coefficients $c_1^{(1)}$ and $c_2^{(1)}$ equal to the exactly calculated values (see Appendix A) and the two remaining ones due to the relations (27) and (28). This approximation gives

$$c_1^{(1)} = 0.70,\ c_2^{(1)} = -0.14,\ c_3^{(1)} = 0.044,\ c_4^{(1)} = -0.0089, \quad (29)$$

so that $\sum c_i^{(1)}\lambda_i^{(1)} = 2.00$ and $\sum c_i^{(1)}(\lambda_i^{(1)})^3 = 16.03$. As shown in Appendix A, the four terms (29) approximate the linear function (26) even better than the twenty exact coefficients $c_i^{(1)}$ not to say that the sum of the first twenty terms of the series (28) results in 84 instead of 16.

As a result, we obtain for the potential $\psi(l)$ as a function of the distance l along the magnetic field line $f = \text{const}$

$$\psi(l) = \frac{1}{2}\frac{\Omega B_0 R_0^2}{c}\cos\chi \times \left[1 - \frac{f}{f_*} - \sum_i c_i^{(0)}\left(\frac{l}{R}\right)^{-\lambda_i^{(0)}/\theta_0} J_0\left(\lambda_i^{(0)}\sqrt{f/f_*}\right)\right] + \frac{3}{8}\frac{\Omega B_0 R_0^3}{cR}\sin\varphi\sin\chi\left[\left(\frac{f}{f_*}\right)^{1/2}\left(1 - \frac{f}{f_*}\right)\left(\frac{l}{R}\right)^{1/2} - \sum_i c_i^{(1)}\left(\frac{l}{R}\right)^{-\lambda_i^{(1)}/\theta_0} J_1\left(\lambda_i^{(1)}\sqrt{f/f_*}\right)\right]. \quad (30)$$

Here we can put $\theta_0 = R_0/R = \text{const}$. Accordingly, the longitudinal electric field $E_\parallel = -\partial\,\psi\,/\partial\,l$ looks like

$$E_\parallel = -\frac{1}{2}\,\frac{\Omega B_0 R_0}{c}\cos\chi\,\times$$
$$\sum_i c_i^{(0)}\lambda_i^{(0)}\left(\frac{r}{R}\right)^{-\lambda_i^{(0)}/\theta_0-1} J_0\left(\lambda_i^{(0)}\theta/\theta_0\right)$$
$$-\frac{1}{4}\,\frac{\Omega B_0 R_0}{c}\,\frac{R_0}{R}\sin\varphi\sin\chi\,\times$$
$$\sum_i c_i^{(1)}\lambda_i^{(1)}\left(\frac{r}{R}\right)^{-\lambda_i^{(1)}/\theta_0-1} J_1\left(\lambda_i^{(1)}\theta/\theta_0\right)$$
$$-\frac{3}{16}\left(\frac{f}{f_*}\right)^{1/2}\left(1-\frac{f}{f_*}\right)\frac{\Omega B_0 R_0^3}{cR^2}\left(\frac{l}{R}\right)^{-1/2}\sin\varphi\sin\chi\,. \tag{31}$$

Here the following points should be stressed.

(i) The expression

$$\psi(r,\theta,\varphi) = \frac{1}{2}\,\frac{\Omega B_0 R_0^2}{c}\left[1-\frac{\theta^2}{\theta_0^2(r)}\right]\cos\chi + \frac{3}{8}\,\frac{\Omega B_0 R_0^2}{c}\left[\theta-\frac{\theta^3}{\theta_0^2(r)}\right]\sin\varphi\sin\chi \tag{32}$$

in (17) is indeed the exact asymptotic solution at large distances from the star surface $(r-R)\gg R_0$ in the dipole magnetic field (certainly, in the limit $\theta\ll 1$).

(ii) At large distances $(r-R)\gg R_0$, the magnetic field lines $\theta(r)\propto r^{1/2}$ become equipotential only for the symmetric component of the potential ψ. For the anti-symmetric (φ-dependent) part realizing for any oblique rotator with $\chi\neq 0^\circ$, the longitudinal electric field decreases on the scale of the star radius R, not the polar cap radius R_0. We emphasize that this effect does not exist for a model of the conical geometry of open magnetic field lines when $\theta_0 = \text{const}$.

(iii) As a result, one can obtain for the anti-symmetric component of the potential

$$\psi(l) = \frac{3}{8}\left(\frac{f}{f_*}\right)^{1/2}\left(1-\frac{f}{f_*}\right)\frac{\Omega B_0 R_0^3}{cR}\left(\frac{l}{R}\right)^{1/2}\sin\varphi\sin\chi\,, \tag{33}$$

where again l denotes the coordinate along the magnetic field line, and we use the dimensionless area $0<f<f_*$. As we see, the additional potential drop within the light cylinder $\psi(l=R_\mathrm{L})$ is the same as the characteristic vacuum potential within the polar cap.

(iv) Accordingly, the additional parallel electric field looks like

$$E_\parallel^{\mathrm{add}} = -\frac{3}{16}\left(\frac{f}{f_*}\right)^{1/2}\left(1-\frac{f}{f_*}\right)\frac{\Omega B_0 R_0^3}{cR^2}\left(\frac{l}{R}\right)^{-1/2}\sin\varphi\sin\chi\,. \tag{34}$$

(v) Previously, no one paid attention to the existence of an additional longitudinal field for the case of an oblique rotator when the dependence of the boundary of the region of open field lines on the distance to the star becomes significant. In particular, in the famous work of Muslimov & Tsygan (1992), a change of variables $\xi = \theta/\theta_0(r)$ was made when solving the equation (11), but in what follows, the dependence $\theta_0(r)$ on r was not taken into account.

2.2 Particle acceleration

The most important result obtained in the previous section is that, for the non-zero inclination angle χ, there is the longitudinal electric field $E_\parallel$ (34) which decreases not on the polar cap scale R_0 but on the scale of the radius r up to the light cylinder. As a result, it produces a significant effect on the motion of particles, which, as is well known, is described by the equation

$$\frac{\mathrm{d}\mathcal{E}_\mathrm{e}}{\mathrm{d}l} = eE_\parallel - \frac{2}{3}\,\frac{e^2}{R_\mathrm{c}^2}\left(\frac{\mathcal{E}_\mathrm{e}}{m_\mathrm{e}c^2}\right)^4. \tag{35}$$

Here R_c is the curvature radius of the magnetic field line. For $\theta\ll 1$ (i.e. for $l\ll R_\mathrm{L}$), one can put

$$R_\mathrm{c} \approx \frac{4}{3}\,f^{-1/2}R_\mathrm{L}^{1/2}l^{1/2}. \tag{36}$$

It should be immediately noted that due to the additional factor R_0/R, this component of the longitudinal electric field becomes significant near the surface of the neutron star for the inclination angles $\cos\chi\sim R_0/R$ only. Fig. 1 shows the values of the Lorentz-factor $\gamma = \mathcal{E}_\mathrm{e}/m_\mathrm{e}c^2$ of a particle accelerated from the surface of a neutron star from the point $f=0.7$ and $\varphi = 90^\circ$ obtained by solving the equation (35) for two values of the pulsar period $P=0.3$ s (upper curves) and $P=1$ s (lower curves) for small ($\chi = 30^\circ$, top) and large ($\chi = 85^\circ$, bottom) inclination angles. The dashed lines show the solutions in which the additional electric field (34) is neglected. As we see, the role of the additional electric field becomes noticeable only for almost orthogonal rotators.

However, for us, it is much more important that for pulsars with relatively large periods $P\sim 1$ s, i.e. just near 'the death line', the energy losses of a particle described by the second term in the equation (35)

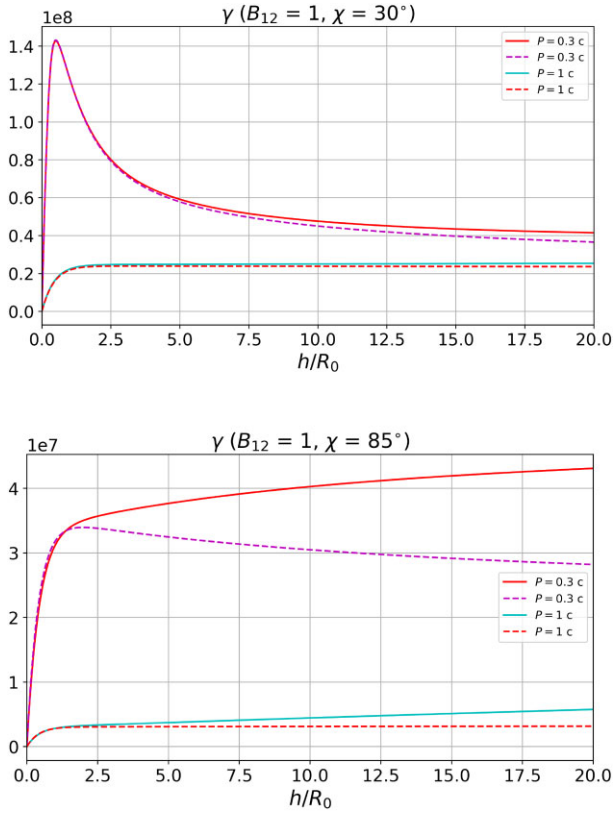

Figure 1. Lorentz-factor $\gamma = \mathcal{E}_\mathrm{e}/m_\mathrm{e}c^2$ of a particle accelerated from the surface of a neutron star obtained by solving the equation (35) for two values of the pulsar period $P=0.3$ s and $P=1$ s for small ($\chi = 30^\circ$, top) and large ($\chi = 85^\circ$, bottom) inclination angles. The dashed lines for each of the two periods show the solutions in which the additional electric field (34) is neglected.

becomes negligible. Therefore, the lower curves in Fig. 1 correspond to the electric potential $\psi(l)$. For this reason, in what follows, for such pulsars, we can simply put $\mathcal{E}_e(l) = e\psi(l) - e\psi(l_0)$, where l_0 corresponds to the particle creation point. For shorter periods P, the particle energy does not reach the maximum possible energy $e\psi$, and subsequently decreases with increasing the distance from the neutron star surface.

2.3 General relativistic correction

As is well known, the effects of general relativity and, in particular, the frame-dragging (Lense-Thirring) effect, under certain conditions, can play a significant role in the generation of secondary plasma near the polar caps of the neutron star (Beskin 1990; Muslimov & Tsygan 1992; Philippov et al. 2015, 2020). For this reason, below, we estimate all possible corrections which can affect the production of secondary particles. For simplicity, we restrict ourselves to only the first order in the small parameter r_g/R, where $r_g = 2GM/c^2$ is the black hole radius.

Starting from the time-independent Maxwell equation in the rotation reference frame (see Thorne, Price & Macdonald 1986 for more detail)

$$\nabla \times (\alpha \boldsymbol{E} + \boldsymbol{\beta} \times \boldsymbol{B} + \boldsymbol{\beta}_R \times \boldsymbol{B}) = 0, \tag{37}$$

where α is the lapse function ($\alpha^2 \approx 1 - r_g/R$), $\boldsymbol{\beta}$ is Lense-Thirring vector and $\boldsymbol{\beta}_R = \boldsymbol{\Omega} \times \boldsymbol{r}/c$, we obtain

$$\alpha \boldsymbol{E} + \boldsymbol{\beta} \times \boldsymbol{B} + \boldsymbol{\beta}_R \times \boldsymbol{B} = -\nabla\psi. \tag{38}$$

For $\rho_e = 0$, this equation gives

$$\nabla\left(\frac{\nabla\psi}{\alpha}\right) = 4\pi\rho_{GJ}, \tag{39}$$

where now the Goldreich–Julian charge density looks like

$$\rho_{GJ} = -\frac{1}{8\pi^2}\nabla_k\left(\frac{\Omega-\omega}{\alpha c}\nabla^k\Psi\right). \tag{40}$$

As we see, the first relativistic correction $(1 - \omega/\Omega)$ appears in the expression for ρ_{GJ}, where the ratio ω/Ω depends on the neutron star moment of inertia $I_r \sim MR^2$:

$$\frac{\omega}{\Omega} = \frac{I_r r_g}{Mr^3}. \tag{41}$$

Thus this correction just corresponds to a small value $\sim r_g/R$ under consideration. To determine the relativistic corrections, we chose the values $M = 1.4\,M_\odot$ for neutron star mass, $R = 12$ km for that radius and $I_r = 150\,\mathrm{M_\odot km^2}$ for the moment of inertia (Greif et al. 2020). Notably, the characteristic scale of the changes in all the relativistic corrections are R, in contrast, the scale of change in ψ is $R_0 \ll R$. Therefore, one can consider all relativistic corrections as constants, i.e. we can put $r = R$ in (41). The second relativistic correction appears in the expression for the magnetic field flux

$$\Psi = 2\pi|\boldsymbol{m}|\frac{\sin^2\theta_m}{r}\left(1+\frac{3}{4}\frac{r_g}{r}\right). \tag{42}$$

As for small angles θ_m, one can put $\sin\theta_m = r_\perp/r$, i.e. to write down

$$x^2 = \frac{\Psi}{2\pi|\boldsymbol{m}|}y^3\left(1+\frac{3}{4}\frac{r_g}{y}\right)^{-1}, \tag{43}$$

where $x = r_\perp$ and $y = r$, we obtain for the curvature radius $R_c \approx 1/y''_{xx}$ the following correction $R_{c,\,GR} = K_{cur}R_c$, where

$$K_{cur} = \left(1-\frac{1}{2}\frac{r_g}{R}\right). \tag{44}$$

Next, for the polar cap radius $R_{0,\,GR} = K_{cap}R_0$, we have

$$K_{cap} = \left(1-\frac{3}{8}\frac{r_g}{R}\right). \tag{45}$$

Finally, equation (39) looks now like

$$\frac{\alpha^2}{r_\perp}\frac{\partial}{\partial r_\perp}\left(r_\perp\frac{\partial\psi}{\partial r_\perp}\right) + \frac{\partial^2\psi}{\partial z^2} = -\frac{2\Omega B_0}{c}\left(1+\frac{3}{4}\frac{r_g}{R}\right)\left(1-\frac{\omega}{\Omega}\right). \tag{46}$$

As a result, we obtain the general relativistic correction for the symmetric potential $\psi_{GR}(r_\perp) = K_\psi\,\psi(r_\perp)$ at distances $h > R_0$ over the star surface as

$$K_\psi = \left(1-\frac{\omega}{\Omega}\right)\left(1-\frac{r_g}{R}\right)^{-1}. \tag{47}$$

Thus, as expected, we can conclude that the effects of general relativity lead to corrections at the level of 10–20 per cent. Consequently, the corresponding corrections at first glance do not go beyond the uncertainty in other quantities, such as, e.g. the radius and moment of inertia of a neutron star. Nevertheless, below, we include general relativity corrections into consideration since, as will be shown, these corrections lead to a significant change in the rate of production of secondary particles.

3 GENERATION OF CURVATURE PHOTONS

3.1 Effective photon energy

The next point, which can be important in the vicinity 'the death line' is the question of the effective energy of the curvature γ-quanta leading to the production of the secondary pairs. Recall that in most cases (see, e.g. Timokhin & Harding 2015), it was assumed that all the photons emitted by the relativistic electron with the energy $\mathcal{E}_e = \gamma_e m_e c^2$ are radiated at the characteristic frequency

$$\omega_c = \frac{3}{2}\frac{c}{R_c}\gamma_e^3, \tag{48}$$

which is larger than the maximum of the energy spectrum $0.29\,\omega_c$ (Landau & Lifshits 1971). Below, we show that the very first pairs are produced by even more energetic photons, whose frequencies are several times higher than the characteristic frequency ω_c (48).

Indeed, the spectrum of the curvature radiation (i.e. the energy radiated in the frequency domain $\mathrm{d}\omega$ at the distance $\mathrm{d}l$)[1]

$$\mathrm{d}I = \frac{\sqrt{3}}{2\pi}\frac{e^2}{cR_c}\gamma_e F(\omega/\omega_c)\mathrm{d}\omega\,\mathrm{d}l, \tag{49}$$

where

$$F(\xi) = \xi\int_\xi^\infty K_{5/3}(x)\mathrm{d}x, \tag{50}$$

$K_{5/3}$ is the Macdonald function, and $\xi = \omega/\omega_c$, has a rather long tail. As a result, although a relativistic particle needs to travel a certain distance l_{rad} for the emission of high-energy photons with $\omega \gg \omega_c$, the free path length l_γ of a γ-quantum before the creation of a secondary electron–positron pair will be much shorter than for the photons radiated near the maximum.

[1]This expression can be easily obtained from a well-known synchrotron spectrum (Landau & Lifshits 1971) by replacing the Larmor radius $r_L = m_e c^2\gamma/eB$ with the curvature radius of the magnetic field line R_c.

Since in what follows, we are only interested in the photons with frequencies $\omega \gg \omega_c$, one can use the following asymptotic behaviour of the Macdonald's function (Abramowitz & Stegun 1965)

$$K_{5/3}(x) \approx \sqrt{\frac{\pi}{2x}}\, e^{-x} \left(1 + \frac{91}{72}\frac{1}{x} + \dots\right), \tag{51}$$

i.e. consider only the two first terms of the expansion in terms of $1/x$. Accordingly, with the same accuracy

$$F(x) \approx \sqrt{\frac{\pi x}{2}}\, e^{-x} \left(1 + \frac{55}{72}\frac{1}{x} + \dots\right). \tag{52}$$

Below, we need a general expression for an arbitrary dependence of the energy $\mathcal{E}_e(l) = \gamma_e(l) m_e c^2$ of the emitting particle on the distance l. Assuming that a photon with the frequency $\omega \gg \omega_c$ can be emitted if the total energy

$$\mathcal{E}_\omega = \frac{\sqrt{3}}{2\pi}\frac{e^2}{cR_c}\int_{l_0}^{l_0+l_{rad}} \int_{\omega}^{\infty} \gamma_e(l) F[\xi(l)]\, d\omega\, dl, \tag{53}$$

radiated above this frequency is equal to photon energy: $\mathcal{E}_\omega = \hbar\omega$. Here, $\xi(l) = (3/2)(c/R_c)\gamma_e^3(l)$, and l_0 is the radiation coordinate. For the constant particle energy $\gamma_e = \text{const}$, we have

$$\mathcal{E}_\omega = \frac{\sqrt{3}}{2\pi}\frac{e^2}{cR_c}\omega_c\, l_{rad}\, \gamma_e \int_{\xi}^{\infty} F(\xi) d\xi. \tag{54}$$

Introducing finally a new variable

$$\xi' = \frac{2}{3}\frac{\omega R_c}{c}\gamma_e^{-3}(l), \tag{55}$$

we obtain

$$\xi = \frac{\sqrt{3}}{2\pi}\frac{e^2}{\hbar c}\int_0^{l_{rad}} \frac{dl}{R_c}\, \gamma_e(0)\frac{\gamma_e^4(l)}{\gamma_e^4(0)} \int_{\xi}^{\infty} F(\xi')\, d\xi', \tag{56}$$

where $\gamma(0) = \gamma(l_0)$ and $\gamma(l_{rad}) = \gamma(l_0 + l_{rad})$. Relation (56) determines implicitly the connection between l_{rad} and ξ. In particular, for $\gamma_e = \text{const}$, we obtain for the radiation length l_{rad}

$$l_{rad} = \sqrt{\frac{8\pi}{3}}\frac{\hbar c}{e^2} R_c\, \gamma_e^{-1}\sqrt{\xi}\left(1 - \frac{91}{72}\frac{1}{\xi} + \dots\right) e^{\xi}. \tag{57}$$

Further, the free path length l_γ of a photon can be written as (Sturrock 1971; Ruderman & Sutherland 1975)

$$l_\gamma = \frac{8}{3\Lambda} R_c \frac{B_{cr}}{B}\frac{m_e c^2}{\hbar\omega_c}\frac{1}{\xi}, \tag{58}$$

where $\Lambda = 15$–20 is the logarithmic factor: $\Lambda \approx \Lambda_0 - 3\ln\Lambda_0$, where

$$\Lambda_0 = \ln\left[\frac{e^2}{\hbar c}\frac{\omega_B R_c}{c}\left(\frac{B_{cr}}{B}\right)^2\left(\frac{m_e c^2}{\mathcal{E}_{ph}}\right)^2\right] \sim 20. \tag{59}$$

Minimizing now the sum $l_{rad} + l_\gamma$ by the value ξ, one can obtain the energy of a photon $\hbar\omega = \xi\hbar\omega_c$ producing the first secondary pair. In particular, for the constant particle energy, we have the following relation to determine the value ξ

$$\xi^{5/2} e^{\xi}\left(1 - \frac{55}{72}\frac{1}{\xi} + \dots\right) = \mathcal{K}, \tag{60}$$

where

$$\mathcal{K} = \frac{4\sqrt{2}}{3\sqrt{3\pi}\,\Lambda}\frac{B_{cr}}{B}\frac{R_c}{a_B}\gamma_e^{-2} \approx 40\, R_{c,7} B_{12}^{-1}\gamma_7^{-2}. \tag{61}$$

Here, $B_{12} = B/(10^{12}\text{ G})$, $R_{c,7} = R_c/(10^7\text{ cm})$, $\gamma_7 = \gamma_e/10^7$, and $a_B = \hbar^2/m_e e^2 = 5.3 \times 10^{-9}$ cm is the Bohr radius. Accordingly, the total length $l_{tot} = l_{rad} + l_\gamma$ in this case looks like

$$l_{tot} = \frac{8}{3\Lambda}\frac{B_{cr}}{B}\frac{m_e c^2}{\xi\hbar\omega_c}\left(1 + \frac{1}{\xi}\right). \tag{62}$$

Table 1. Tabulation of the inverse function $\xi(\mathcal{K})$ (60).

$\mathcal{K}$	30	100	300	10^3	$3\cdot10^3$	10^4	$3\cdot10^4$	10^5
ξ	2.1	2.6	3.1	3.8	4.5	5.2	6.0	6.8

Table 2. Values $\mathcal{K}$ and ξ for some pulsars located within 'the death valley'. The pulsar parameters are taken from the ATNF catalog (Manchester et al. 2005).

PSR	P (s)	$\dot{P}_{-15}$	B_{12}	$\mathcal{K}$	ξ
J0250 + 5854	23.5	27.1	25	3.3×10^4	6.1
J0418 + 5732	9.01	4.10	6.1	3.2×10^4	6.1
J1210 − 6550	4.24	0.43	1.3	1.0×10^5	6.8
J1333 − 4449	0.46	0.0005	0.016	3.3×10^6	9.5
J2144 − 3933	8.51	0.50	2.1	6.6×10^5	8.2
J2251 − 3711	12.1	13,1	12.5	1.4×10^4	5.5

As shown in Table 1, even for the characteristic parameters, the most effective frequency $\omega = \xi\omega_c$ is indeed higher than ω_c (48). As for the pulsars located within 'the death valley', their effective frequency can be sufficiently higher. In Table 2, we show the parameters $\mathcal{K}$ and ξ for some of these pulsars. Their parameters were taken from the ATNF catalog (Manchester et al. 2005), and the appropriate Lorentz-factors correspond to the potential drop ψ (30). As we see, for all these pulsars, the effect under consideration can indeed play a significant role. A detailed analysis of all the pulsars located within 'the death valley' will be provided in Paper II.

3.2 Free pass

When determining the value of ξ, the accuracy in determining the logarithmic factor Λ is insignificant since equation (60) actually gives $\xi \sim \ln K$. On the other hand, near 'the death line', more accurate determination of the free path-length l_γ is necessary. This, in particular, is due to the fact that l_γ turns out to be comparable with the radius of the star R, i.e. with the scale at which the magnetic field of the neutron star decreases significantly; this was not taken into account when deriving equation (47). For this reason, to determine the path length of a photon, we will use the exact expression for the probability w_l of the photon production at a length dl (Berestetsky, Lifshits & Pitaevsky 1971)

$$dw_l = \frac{3\sqrt{3}}{16\sqrt{2}}\frac{e^3 B\sin\theta_b}{\hbar m_e c^3}\exp\left(-\frac{8}{3}\frac{B_{cr}}{B(l)\sin\theta_b(l)}\frac{m_e c^2}{\mathcal{E}_{ph}}\right) dl, \tag{63}$$

where again $B_{cr} = m_e^2 c^3/e\hbar \approx 4.4\times10^{13}$ G is the critical magnetic field, and θ_b is the angle between the magnetic field $\boldsymbol{B}$ and the wave vector $\boldsymbol{k}$. As a result, the free pass length l_γ should be determined from the condition

$$\int_0^{l_\gamma} dw_l = 1. \tag{64}$$

In conclusion, we note one more convenience of using the parameter Λ. Indeed, since in a not very strong magnetic field $B_0 \sim 10^{12}$ G, secondary particles at the time of birth move at the angle $\theta \sim l_\gamma/R_c$ to the magnetic field lines, while their energy $\gamma m_e c^2$ is to be one half of the energy of the curvature photon $\hbar\omega_{cur}$ (Beskin 1982; Daugherty & Harding 1983), the ratio of the characteristic frequency

of a synchrotron photon $\omega_{\rm syn} = (3/2)\theta\omega_B\gamma^2$ to the frequency of a curvature photon $\omega_{\rm cur}$

$$\frac{\omega_{\rm syn}}{\omega_{\rm cur}} = \frac{3}{8}\frac{B_0}{B_{\rm cr}}\frac{\hbar\,\omega_{\rm cur}}{m_{\rm e}c^2}\frac{l_\gamma}{R_{\rm c}} \tag{65}$$

turns out to be exactly Λ^{-1}. Just for this reason, as was already mentioned above, free path length of synchrotron photons is to be 15–20 times larger than free path length of the curvature photons. Therefore, near 'the death line', the role of synchrotron photons should not be significant.

4 GENERATION OF SECONDARY PAIRS

4.1 Outflow

In general, we follow the approach developed by Hibschman & Arons (2001). The main difference is that we analyse the dependence of the number density of secondary particles $n_\pm$ on the distance $r_\perp$ from the magnetic axis rather than the energy spectrum.

Let us consider one primary particle moving along the magnetic field line intersecting the star surface at the distance r_0 from the axis. It produces dN curvature photons in the frequency domain dω at the path dh

$$\mathrm{d}N = \frac{\sqrt{3}}{2\pi}\frac{e^2}{cR_{\rm c}(h)}\frac{\gamma_{\rm e}F(\omega/\omega_{\rm c})}{\hbar\omega}\mathrm{d}\omega\,\mathrm{d}h. \tag{66}$$

On the other hand, frequency ω determines the free path $l_\gamma = l_\gamma(\omega)$ which, in turn, determines the magnetic field line at which the secondary pair is created

$$r_\perp = \left(1 - \frac{3}{8}\frac{l_\gamma^2}{R^2}\right) r_0, \tag{67}$$

where again $r_\perp$ is the distance from the axis at the star surface, and h is the height of the γ-quanta emission. Note that in a dipole magnetic field, this expansion does not contain the corrections $\propto hl_\gamma/R^2$ (and, certainly, it does not contain the term $\propto h^2/R^2$ as $r_\perp = r_0$ for $l_\gamma = 0$).

As we show below, the leading term in (67) is enough for our consideration. On the other hand, in what follows, to determine with the required accuracy the exponent in the pair creation probability $w_l(\theta_{\rm b})$ (63), we use the exact expression for the angle $\theta_{\rm b}$ between the magnetic field $\boldsymbol{B}$ and the wave vector $\boldsymbol{k}$. In a dipole magnetic field, for γ-quanta radiated tangentially at the height h, it looks like

$$\theta_{\rm b} = \frac{3}{4}\frac{r_0 l_\gamma}{R^2} f(h), \tag{68}$$

where the correction function $f(h)$ for $\theta_{\rm b} \ll 1$ is

$$f(h) = \left(1 + \frac{h}{R}\right)^{1/2}\left(1 + \frac{\mathcal{L}(h)l_0}{R} + \frac{h}{R}\right)^{-1}. \tag{69}$$

Here, we introduce by definition another correction function $\mathcal{L}(h)$ as

$$l_\gamma(l_0, h) = \mathcal{L}(h)\,l_0, \tag{70}$$

where

$$l_0(\omega) = \frac{32}{9\Lambda}\frac{R^2}{r_0}\frac{B_{\rm cr}}{B_0}\frac{m_{\rm e}c^2}{\hbar\omega} \tag{71}$$

is the γ-quantum free pass length in the case $l_\gamma \ll R$ with the starting point $h = 0$. The coefficient $\mathcal{L}(h)$ due to the strong non-linearity of the problem for $h \sim l_0 \sim R$ should be determined numerically by direct integration (64)

$$\int_0^{l_\gamma} w_l(h)\,\mathrm{d}l = 1 \tag{72}$$

Table 3. Tabulation of the function $\mathcal{L}(x_0, x_\perp, h)$ (70) for $x_0 = 0.6$ and for different values $x_\perp$.

h/R	0.0	0.1	0.2	0.3	0.4	0.5	0.6	0.7
0.599	1.0	1.4	1.9	2.6	3.4	4.3	5.4	6.7
0.59	1.5	2.0	2.7	3.4	4.3	5.4	6.6	8.1
0.58	1.9	2.5	3.3	4.1	5.1	6.3	7.7	9.3

for probability $w_l(h)$ corresponding to the starting point h at which the photon free pass length is equal to l_γ (see Table 2). Certainly, $\mathcal{L} \to 1$ for $h \to 0$ and $l_\gamma \to 0$ ($r_\perp \to r_0$). Finally, for the primary particle moving along the magnetic field line, we have

$$R_{\rm c} = \frac{4}{3}\frac{R^2}{r_0}\left(1 + \frac{h}{R}\right)^{1/2}. \tag{73}$$

As a result, one can write down for the $r_\perp$ distribution of the secondary particles as

$$\mathrm{d}N = \frac{\sqrt{3}}{2\pi}\frac{e^2}{\hbar c}\frac{\gamma_{\rm e}F(\omega/\omega_{\rm c})}{R_{\rm c}\omega}\frac{\mathrm{d}\omega}{\mathrm{d}r_\perp}\mathrm{d}r_\perp\,\mathrm{d}h. \tag{74}$$

To determine the derivative dω/d$r_\perp$, one can rewrite the relation (67) as

$$\frac{l_\gamma(\omega)}{R} = \frac{2\sqrt{2}}{\sqrt{3}}\frac{(r_0 - r_\perp)^{1/2}}{r_0^{1/2}}. \tag{75}$$

It finally gives

$$\frac{1}{\omega}\frac{\mathrm{d}\omega}{\mathrm{d}r_\perp} = \frac{1}{2(r_0 - r_\perp)}\left(1 - \frac{\omega}{\mathcal{L}}\frac{\mathrm{d}\mathcal{L}}{\mathrm{d}\omega}\right)^{-1}. \tag{76}$$

Within approximation (67) we consider, the value of $\mathcal{L}$ does not depend on ω (both free path lengths l_0 and l_γ are mainly determined by the exponent, which both depend on ω as ω^{-1}); therefore, below, we do not take into account the logarithmic derivative $\omega/\mathcal{L}(\mathrm{d}\mathcal{L}/\mathrm{d}\omega)$.

As a result, we obtain for the linear distribution of secondary particle $n_\pm\,\mathrm{d}x_\perp$ creating by one primary particle moving along the magnetic field line with a foot point distance from the axis r_0

$$n_\pm(r_\perp) = \frac{3\sqrt{3}}{16\pi}\frac{e^2}{\hbar c}\frac{R_0}{R}\frac{x_0}{(x_0 - x_\perp)}\int_0^H \frac{\mathrm{d}h}{R}\gamma_{\rm e}(x_0, h)F(\xi), \tag{77}$$

where now

$$\xi = \frac{64\sqrt{2}}{27\sqrt{3}\Lambda}\frac{B_{\rm cr}}{B_0}\frac{R^3}{\lambda R_0^2}\frac{(1 + h/R)}{\gamma_{\rm e}^3(x_0, h)}\frac{\mathcal{L}(x_0, x_\perp, h)}{x_0\sqrt{x_0}\sqrt{x_0 - x_\perp}}. \tag{78}$$

Here, we introduce by definition two dimensionless parameters

$$x_0 = \frac{r_0}{R_0}; \qquad x_\perp = \frac{r_\perp}{R_0}. \tag{79}$$

As for the upper integration limit H, it can be set equal to infinity, since, as shown in Table 3, the parameter $\mathcal{L}$ introduced above increases rapidly with increasing h. Therefore, already at $h \sim H$, the integrand becomes exponentially small due to the large value of the argument ξ (78).

In Fig. 2, we show secondary particle distributions $n_\pm(r_\perp)$ (77) generated by single primary particles with the starting points $x_0 = 0.4$, $x_0 = 0.6$, and $x_0 = 0.8$ for $P = 1$ s, $B_{12} = 1$, and $\chi = 0°$. The energy of the primary particles $\mathcal{E}_{\rm e} = \gamma_{\rm b}m_{\rm e}c^2$ was determined from the vacuum potential ψ (30). As we see, even though the maximum of the distribution $n_\pm(r_\perp)$ lies near r_0 (i.e. the corresponding secondary particles are born on practically the same field line as the primary particle), this distribution slowly decreases with increasing distance $r_0 - r_\perp$. Consequently, with the parameters considered here, which

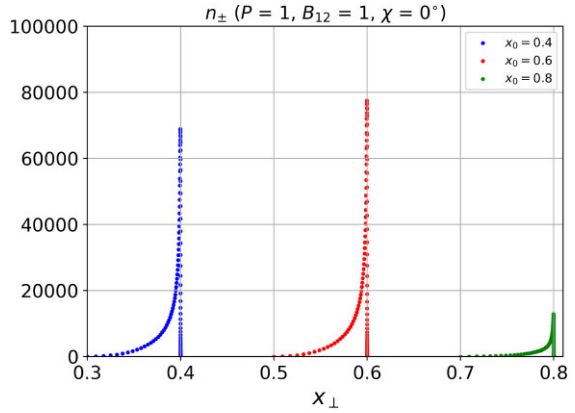

Figure 2. Secondary particle distribution $n_\pm(r_\perp)$ (77) generated by a single primary particle with the starting points $x_0 = 0.4$, $x_0 = 0.6$, and $x_0 = 0.8$ for $P = 1$ s, $B_{12} = 1$, and $\chi = 0°$.

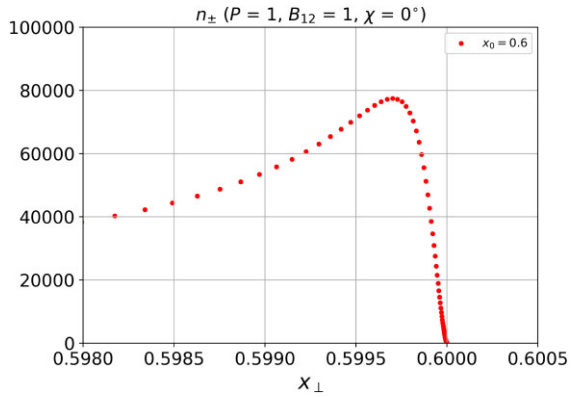

Figure 3. Secondary particle distribution $n_\pm(r_\perp)$ (77) generated by a single primary particle with the starting points $x_0 = 0.6$ near the threshold $x_\perp = x_0$.

are close to 'the death line', a significant part of the secondary particles will be produced at distances h, comparable to the radius of the star R. That is why we do not consider further the production of secondary plasma associated with the synchrotron radiation of secondary particles.

On the other hand, it is clear that $n_\pm = 0$ for $x_\perp = x_0$. As for the position of the maximum in the distributions $n_\pm$, they can be easily determined by setting argument (78) as $\xi = 1$ so that $F(\xi)$ becomes exponentially small for $\xi > 1$. Moreover, using the potential ψ (30) to determine γ_b, one can write down the condition $\xi = 1$ as

$$(x_0 - x_\perp) = x_0^{-3}\mathcal{A}, \tag{80}$$

where

$$\mathcal{A} = \frac{2^7}{3^9\,\Lambda^2}\,\frac{B_{cr}^2}{B_0^2}\,\frac{R^6}{\lambda\!\!\!^{-2} R_0^4}\gamma_b^{-6} \approx 6\times 10^{-5} P^{14} B_{12}^{-8}. \tag{81}$$

Here, we took into account that $\mathcal{L} \approx 1$ for $x_\perp \to x_0$. Therefore, for $P = 1$ s and $B_{12} = 1$ (and for $x_0 = 0.6$), we obtain $x_0 - x_{max} \approx 0.003$. As shown in Fig. 3, this evaluation is in good agreement with our numerical result. Using now relation (75), we obtain that the smallest free path length

$$l_{\gamma,\min} = \frac{2\sqrt{2}}{\sqrt{3}}\,\frac{\mathcal{A}}{x_0^2}\,R \tag{82}$$

corresponds to $0.01\,R \sim R_0$.

Finally, Table 4 shows how the multiplicity λ (i.e. the total number of secondary particles $n_e = n_+ + n_-$ per one primary particle) depends on the position $r_0 = x_0 R_0$. As one can see, taking into account the effects of general relativity leads to a significant (by several times) increase in the production rate of secondary particles. Therefore, it seems necessary to include the effects of general relativity in the consideration of the processes of the production of secondary particles near 'the death line'.

Table 4. Multiplicity λ for $P = 1$ s, $B_{12} = 1$, and $\chi = 30°$.

x_0	0.1	0.2	0.3	0.4	0.5	0.6	0.7	0.8	0.9
λ	0	36	157	305	382	350	209	42	0
λ_{GR}	7	173	498	829	995	1040	663	220	3

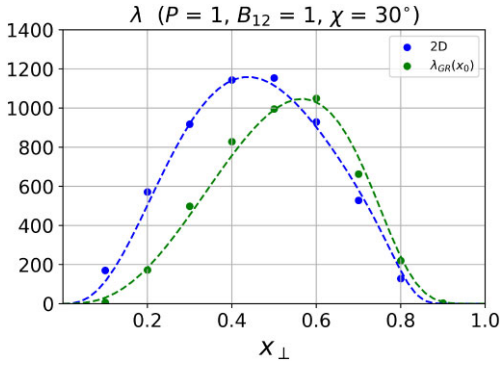

Figure 4. 2D distribution of secondary particle multiplicity $\lambda(x_\perp) = (n_+ + n_-)/n_{prim}$ (84) generated by the homogeneous primary particle distribution $n_{prim} = 1$ for an ordinary pulsar ($P = 1$ s, $B_{12} = 1$, $\chi = 30°$). The right shifted distribution corresponds to multiplicity $\lambda_{GR}(x_0)$ presented in Table 4.

As was already mentioned above, the beginning of the cascade can be initiated by the cosmic gamma background producing 10^5–10^8 primary particles per second in the polar cap region (Shukre & Radhakrishnan 1982). If the primary particles have 2D spatial distribution $dN_{prim} = n_{prim}(r_0, \varphi) r_0 dr_0 d\varphi$, we obtain for the 2D number density of the secondary pairs $n_\pm(r_\perp, \varphi)$

$$n_\pm = \frac{\sqrt{3}}{2\pi}\,\frac{e^2}{\hbar c}\int_{r_\perp}^{R_0} r_0 dr_0 \int_0^H dh\,\frac{\gamma_e F(\omega/\omega_c)}{R_c \omega r_\perp}\,\frac{d\omega}{dr_\perp} n_{prim}. \tag{83}$$

Finally we obtain for $n_\pm(r_\perp, \varphi)$

$$n_\pm = \frac{3\sqrt{3}}{16\pi}\,\frac{e^2}{\hbar c}\,\frac{R_0}{R}\int_{x_\perp}^1 \frac{x_0^2 dx_0}{x_\perp(x_0 - x_\perp)}\int_0^H \frac{dh}{R}\,\gamma_e(x_0, h) F(\xi) n_{prim}. \tag{84}$$

In Fig. 4, we show the 2D distribution of the effective secondary particle multiplicity $\lambda(x_\perp) = (n_+ + n_-)/n_{prim}$ (84) generated by the primary particles with the homogeneous distribution $n_{prim} = 1$ for an ordinary pulsar ($P = 1$ s, $B_{12} = 1$, $\chi = 30°$). The right shifted distribution corresponds to the multiplicity $\lambda_{GR}(x_0)$ presented in Table 4. The fitting curves for $x_\perp \ll 1$ correspond to asymptotic behaviour $n_\pm \propto x_\perp^3$ (see Andrianov et al., in preparation), which, as we see, are satisfied with good accuracy. As expected, the 2D distribution $\lambda(x_\perp)$ is shifted left relative to the distribution $\lambda_{GR}(x_0)$, since, as was shown in Fig. 2, secondary particles are born closer to the magnetic axis compared to the position of the primary particle ($x_\perp < x_0$).

4.2 Inflow

Let us note straight away two essential circumstances. At first, for the formation of a particle production cascade, secondary electron–positron pairs corresponding to the most energetic γ-quanta must be produced in the region of a sufficiently strong longitudinal electric field $E_\parallel$ so that one of the produced particles can stop and then be accelerated in the opposite direction (i.e. inwards to the star surface). For ordinary pulsars, this occurs at distances from the star's surface $h \ll R_{\rm cap}$, where the very existence of a longitudinal electric field is beyond doubt (Ruderman & Sutherland 1975; Arons 1982).

However, near 'the death line', the free path length l_γ of γ-quanta propagating outwards become much larger than the size of the polar cap. Therefore, secondary particles begin to be born at the distances from the star surface $h \gg R_{\rm cap}$ where the longitudinal electric field, as was previously assumed, practically vanishes. However, as was shown, in a real dipole geometry, the longitudinal electric field also exists at large distances. It turns out that such an additional longitudinal field $E_\parallel^{\rm add}$ (34) is sufficient to stop the particles at the distances $h \sim R$ from the star surface.

Indeed, as one can easily show by passing to a reference frame in which γ-quantum propagates perpendicular to the external magnetic field, after an almost instantaneous transition to the lower Landau level, the energy of the secondary particles can be written as $\gamma_\pm m_{\rm e}c^2$, where $\gamma_\pm = \theta_{\rm b}^{-1}$, i.e.

$$\gamma_\pm \sim \frac{R_c}{l_\gamma}. \tag{85}$$

Therefore, before stopping, one of the secondary particles must pass the length

$$\delta l = \frac{\gamma_\pm m_{\rm e}c^2}{eE_\parallel}. \tag{86}$$

It gives

$$\frac{\delta l}{R} \sim \frac{R_{\rm c}}{l_\gamma}\frac{m_e c^2}{eE_\parallel R} \approx A^{-1}\frac{R}{l_\gamma}\frac{R^2c^2}{\Omega\omega_B R_{\rm cap}^4}\left(\frac{l}{R}\right)^{1/2}, \tag{87}$$

where $A = 3/16(f/f_*)(1-f/f_*) \approx 0.1$, $\omega_B = eB_0/m_{\rm e}c$, and we used the relation $R_{\rm c} \approx R/R_{\rm cap}(f/f_*)^{-1/2}$. As a result, we obtain

$$\frac{\delta l}{R} \sim A^{-1}\frac{R}{l_\gamma}\frac{c}{\omega_B R}\left(\frac{\Omega R}{c}\right)^{-3} \sim 10^{-2}P^3 B_{12}^{-1}, \tag{88}$$

so that the stop length δl is, indeed, much less than the free pass length $l_\gamma \sim R$. Therefore, in what follows, we assume that one of the secondary particles begins its reverse motion at the point of its birth.

Here, however, one should pay attention to the fact that the additional longitudinal electric field $E_\parallel^{\rm add}$ works effectively only on that part of the polar cap which is located closer to the rotation axis ($\sin\varphi > 0$ for $\chi < 90^\circ$ and $\sin\varphi < 0$ for $\chi > 90^\circ$). In the other parts of the open field lines, where the opposite inequalities are made, the direction of the additional longitudinal electric field will be opposite to the electric field near the star surface. In particular, for $\sin\varphi = 0$, there is no additional longitudinal electric field $E_\parallel^{\rm add}$ at all.

Finally, we note one more circumstance which significantly distinguishes the processes of pair creation by γ-quanta moving towards the star compared to the case of moving from the star's surface considered above. The point is that, as shown in Fig. 1, the particles moving from the surface of a star are accelerated on a scale $R_0 \ll R$, so that the free path length of γ-quanta can be comparable to the radius of the star. On the other hand, the particles moving towards the star gain most of the energy only near the very surface. Therefore, the free path length of γ-quanta should be of the order of R_0.

As was shown above, the energy of the particles $\mathcal{E}(h)$ moving towards the star can be written with good accuracy in the form

$$\mathcal{E}(h) = e\,\delta\psi(h), \tag{89}$$

where, according to (30),

$$\delta\psi(h) = \frac{1}{2}\frac{\Omega B_0 R_0^2}{c}\mathcal{P}(r_m,\varphi_m)f(h). \tag{90}$$

Here,

$$\mathcal{P}(r_m,\varphi_m) = \left(\cos\chi + \frac{3}{4}\frac{r_m}{R}\sin\chi\cos\varphi_m\right)\left(1-\frac{r_m^2}{R_0^2}\right), \tag{91}$$

and

$$f(h) \approx \exp\left(-\lambda_1 h/R_0\right), \tag{92}$$

where $\lambda_1 \approx 2.5$. The ability to replace the sum of the power functions $(r/R)^{-\lambda/\theta_0}$ in (17) with the exponential term $\exp(-\lambda_1 h/R_0)$ is shown in Fig. A3.

Using the expression for the free pass length l_γ (58) with the energy of the curvature γ-quanta

$$\hbar\omega_{\rm c} = \frac{3}{2}\xi\frac{\hbar c}{R_{\rm c}}\left(\frac{\mathcal{E}(h)}{m_{\rm e}c^2}\right)^3 \tag{93}$$

and the correction factor ξ from (56), we can finally write down the condition of the pair creation over the star surface

$$l_\gamma(h) < h, \tag{94}$$

which can be rewritten as

$$x > \mathcal{B}\exp(3\lambda_1 x). \tag{95}$$

Here $x = h/R_0$,

$$\mathcal{B} = \frac{2048}{81\Lambda\xi f_*^{9/2}}\frac{R^2}{\lambda^2}\frac{c^4}{\omega_B^4 R^4}\frac{1}{x_0^2}\left(\frac{\Omega R}{c}\right)^{-15/2}\mathcal{P}^{-3}, \tag{96}$$

and we again use standard definition (15) for the dimensionless polar cap area f_*. If inequality (94) is violated, then the free path length l_γ becomes greater than the height above the surface of the neutron star h at which it was generated. In this case, γ-quantum does not have time to give birth to a pair before it collides with the surface.

As a result, the condition in which secondary particles will be produced both for the primary particles accelerated from the stellar surface and for the opposite motion) can be written down as[2]

$$\mathcal{B} < 0.05, \tag{97}$$

which gives the following evaluation for the maximum period $P_{\rm max}$

$$P_{\rm max} = 0.8\,B_{12}^{8/15}x_0^{4/15}\mathcal{P}^{2/5}\,s. \tag{98}$$

A value of 0.8 s corresponds to $R = 12$ km, $\Lambda = 15$, $\xi = 3$ and $f_* = 1.6$. As one can see, a rather strong dependence of the limiting period $P_{\rm max}$ on the magnetic field B_{12} makes it easy to explain the observed periods in the range of several seconds. A detailed study of this issue, as was already noted, will be carried out in Paper II.

5 DISCUSSION

Thus, in this Paper I, the first step was taken in a consistent analysis of the conditions leading to the cessation of the secondary pair

[2]When $\mathcal{B} = 0.05$, we have a single root at $h = 0.13\,R_0$.

production for a sufficiently large rotation period P (which, in turn, leads to the termination of radio emission). As is well known, in reality, we have not 'the death line', but 'the death valley' on the $P - \dot{P}$ diagram, which, apparently, is related to the tail of the distribution on some physical parameters. What parameters determine this band will be the subject of Paper II.

As for Paper I, we started from our main assumption that near 'the death line', the polar regions are almost completely free of plasma. This made it possible to accurately determine the potential drop in the area of open field lines. In particular, it was shown that in a dipole magnetic field in the region of open field lines, there is a longitudinal electric field which can stop secondary particles even at sufficiently large distances $h \sim R$ from the surface of the star. To date, this property has not been known.

In addition, the corrections related to the effects of general relativity were determined. As expected, they turned out to be at the level of 10–20 per cent, i.e. at the same level of uncertainty which can be assumed in other quantities, such as the radius and moment of inertia of a neutron star. Nevertheless, due to the strong dependence of the production rate on the energy of primary particles, taking into account the effects of general relativity leads to a significant (several times) increase in the multiplicity of particle production λ. Therefore, in this work, they were included into consideration. Looking into the future, we immediately note that it can be expected that the spread in such quantities as the radius of the star R and the size of the polar cap R_0 (and, certainly, the curvature radius of magnetic field lines R_c) should also lead to a noticeable expansion of 'the death line'. Paper II will be devoted to the analysis of all these issues.

Further, the question of the spatial distribution of the secondary particles produced by curvature photons was investigated in detail (as to synchrotron photons, we assume that near 'the death line', they are not efficient in the production of secondary pairs). First of all, it was shown that a certain role in the production of secondary plasma can play γ-quanta, the energy of which is several times higher than the energy of the maximum of the spectrum $0.44(\hbar c/R_c)\gamma^3$. This effect becomes especially important for the curvature γ-quanta propagating towards the neutron star surface. As a result, conditions (98) for the termination of the cascade were formulated quantitatively. A detailed analysis of the dependence of 'the death line' both on the parameters of a neutron star and on the possible existence of a non-dipole magnetic field is to be carried out in Paper II.

ACKNOWLEDGEMENTS

Authors thank Ya.N.Istomin and A.A.Philippov for useful discussions. This work was partially supported by Russian Foundation for Basic Research (RFBR), grant 20-02-00469.

DATA AVAILABILITY

The data underlying this work will be shared on reasonable request to the corresponding author.

REFERENCES

Abramowitz M., Stegun I. A., 1965, Handbook of mathematical functions. Dover Publications, Inc., New York, p. 378
Arendt P. N., Eilek J. A., 2002, ApJ, 581, 451
Arons J., 1982, ApJ, 254, 713
Arons J., 1993, ApJ, 408, 160
Asseo E., Khechinashvili D., 2002, MNRAS, 334, 743
Barsukov D. P., Tsygan A. I., 2010, MNRAS, 410, 1077
Berestetsky L. D., Lifshits E. M., Pitaevsky L. P., 1971, Quantum Electrodynamics. Pergamon Press, Oxford, p. 386
Beskin V. S., 1982, Astrophys., 18, 266
Beskin V. S., 1990, Sov. Astron. Lett., 16, 286
Beskin V. S., 2010, MHD Flows in Compact Astrophysical Objects. Springer, Berlin, p. 89
Beskin V. S., Gurevich A. V., Istomin I. N., 1983, Sov. J. Exp. Theor. Phys., 58, 235
Bilous A. V. et al., 2019, ApJ, 887, L23
Blandford R. D., Scharlemann E. T., 1976, MNRAS, 174, 59
Cerutti B., Philippov A. A., Spitkovsky A., 2016, MNRAS, 457, 2401
Chen K., Ruderman M., 1993, ApJ, 402, 264
Daugherty J. K., Harding A. K., 1982, ApJ, 252, 337
Daugherty J. K., Harding A. K., 1983, ApJ, 273, 761
Faucher-Giguére C.-A., Kaspi V. M., 2006, ApJ, 643, 2401
Goldreich P., Julian W. H., 1969, ApJ, 157, 869
Gralla S. E., Lupsasca A., Philippov A., 2017, ApJ, 851, 137
Greif S. K., Hebeler K., Lattimer J. M., Pethick C. J., Schwenk A., 2020, ApJ, 901, 155
Gurevich A. V., Istomin I. N., 1985, Sov. J. Exp. Theor. Phys., 62, 1
Hibschman J. A., Arons J., 2001, ApJ, 546, 382
Igoshev A. P., Elfritz J. G., Popov S. B., 2016, MNRAS, 462, 3689
Istomin Y. N., Sobyanin D. N., 2007, Astron. Lett., 33, 660
Konar S., Deka U., 2019, J. Astrophys. Astron., 40, 42
Landau L. D., Lifshits E. M., 1971, The Classical Theory of Fields. Pergamon Press, Oxford, p. 197
Lorimer D. R., Kramer M., 2012, Handbook of Pulsar Astronomy. Cambridge University Press, Cambridge, p. 79
Lyne A., Graham-Smith F., 2012, Pulsar Astronomy. Cambridge University Press, Cambridge, p. 213
Manchester R. N., Hobbs G. B., Teoh A., Hobbs M., 2005, ApJ, 129, 1993
Medin Z., Lai D., 2010, MNRAS, 406, 1379
Michel F. C., 1973, ApJ, 180, 207
Muslimov A. G., Tsygan A. I., 1992, MNRAS, 255, 61
Philippov A., Timokhin A., Spitkovsky A., 2020, Phys. Rev. Lett., 124, 245101
Philippov A. A., Spitkovsky A., Cerutti B., 2015, ApJ, 801, L19
Ruderman M. A., Sutherland P. G., 1975, ApJ, 196, 51
Shukre C. S., Radhakrishnan V., 1982, ApJ, 258, 121
Sturrock P., 1971, ApJ, 164, 529
Thorne K. S., Price R. H., Macdonald D. A., 1986, Black holes: The membrane paradigm. Yale University Press, New Haven, p. 83
Timokhin A. N., 2010, MNRAS, 408, L41
Timokhin A. N., Arons J., 2013, MNRAS, 429, 20
Timokhin A. N., Harding A. K., 2015, ApJ, 810, 144
Usov V. V., Melrose D. B., 1995, Aust. J. Phys., 48, 571
Zhang B., Harding A. K., Muslimov A. G., 2000, ApJ, 531, L135

APPENDIX A: APPROXIMATION BY BESSEL FUNCTIONS

In this Appendix, we illustrate various aspects related to series expansion in the Bessel functions discussed in Section 1. In Figs A1–A2, we show how the expansions in Bessel functions (18) and (21) approximate the functions $1 - x^2$ and $x - x^3$. The top panels show an approximation when we restrict ourselves to only the first four terms c_i (25) and (29), for which the coefficients c_1 and c_2 coincide with the precisely calculated values

$$c_i^{(0)} = \frac{2}{J_1^2(\lambda_i^{(0)})} \int_0^1 x(1-x^2) J_0(\lambda_i^{(0)} x) \mathrm{d}x, \tag{A1}$$

$$c_i^{(1)} = \frac{2}{J_2^2(\lambda_i^{(1)})} \int_0^1 x(x-x^3) J_1(\lambda_i^{(1)} x) \mathrm{d}x, \tag{A2}$$

and the two remaining ones are selected to satisfy relations (18) and (21). Accordingly, the approximations by the first twenty terms of

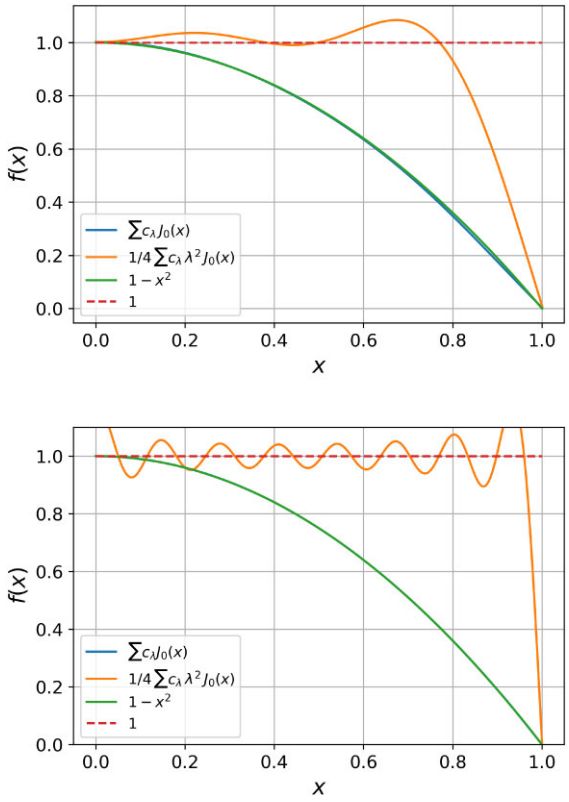

Figure A1. Expansion of the function $1 - x^2$ by Bessel functions $J_0(\lambda_i^{(0)} x)$ (18) using our four terms $c_i^{(0)}$ (25) (top) and the first exact twenty terms (A1) (bottom). The degree of agreement of the second derivative (23) is also shown.

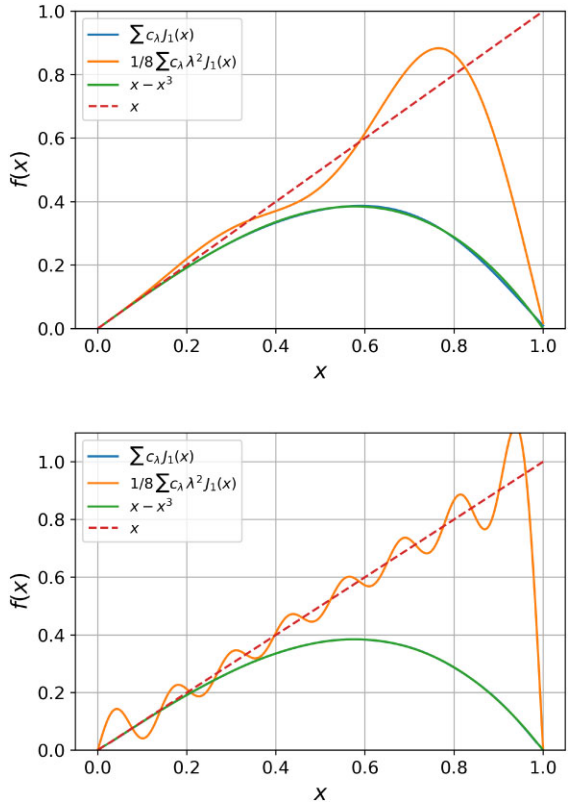

Figure A2. Expansion of the function $x - x^3$ by Bessel functions $J_1(\lambda_i^{(1)} x)$ (21) using our four terms $c_i^{(1)}$ (29) (top) and the first exact twenty terms (A2) (bottom). The degree of agreement of the second derivative (26) is also shown.

the series are shown in the bottom panels. As we see, both series reproduce the functions $1 - x^2$ and $x - x^3$ with high accuracy. As for their second derivatives (23) and (26), in some respects, our first four terms approximate these functions even better than twenty exact terms.

Finally, in Fig. A3, we present the comparison of the dimensionless parallel component of the electric field $E_\parallel = -(\nabla\psi\mathbf{B})/B/(\psi_0/R_0)$ calculated for cylindrical and conical geometries for $P = 1$ s, $B_{12} = 1$, and $\chi = 0^\circ$. As we can see, although in the first case, the expansion is carried out in exponential functions $e^{-\lambda_i z}$, and for dipole geometry in power-law dependencies $(r/R)^{-\lambda_i/\theta_0}$, their difference becomes indistinguishable already for four first terms of the series. Moreover, good enough agreement is achieved using only the first exponential term (dash line). In turn, this confirms the possibility to write down the condition for the presence of a cascade of secondary plasma production (i.e. the condition that secondary particles will be produced both for primary particles

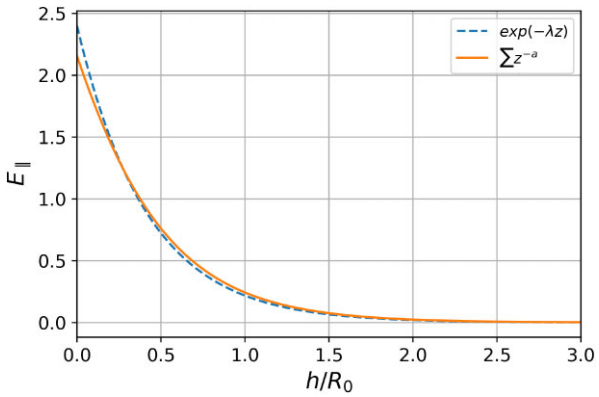

Figure A3. Dimensionless parallel electric field $E_\parallel$ as a function of $z = h/R_0$ determined by a power series (17) (solid line) and by one single exponential term (92) (dashed line).

accelerated from the stellar surface and for the opposite motion) as (107).

This paper has been typeset from a TEX/LATEX file prepared by the author.